Int. J. Multiphase Flow Vol. 14, No. 5, pp. 547–564, 1988
Printed in Great Britain.

0301-9322/88 $3.00 + 0.00

FLOW OF BUBBLES THROUGH NOZZLES

J. T. KUO† and G. B. WALLIS
Thayer School of Engineering, Dartmouth College, Hanover, NH 03755, U.S.A.

(*Received* 24 *September* 1987; *in revised form* 27 *April* 1988)

Abstract—One of the fundamental objectives in the mathematical modeling of two-phase flow is to understand and to formulate the interaction forces between two phases. For this purpose a well-defined two-phase flow situation, flow of bubbles through nozzles, was set up in the laboratory. A range of liquid flow fields was set up by flowing water through nozzles. Individual bubbles were injected into the water stream and their trajectories were recorded to provide data for evaluation and comparison with theories.

Because of the limitations of the conventional photographic method of recording the bubble path, a computer-based optical system was designed for fast data acquisition. The optical system works on the principle of the interruption of a light beam by a bubble passing between a sheet of light and a row of phototransistors. The bubble position (horizontal as well as vertical) along the nozzle is determined by its crossing through the light path to several rows of phototransistors attached to the nozzle. The performance and accuracy of the optical system were tested under various known physical situations. All the tests showed that the optical system is competent and effective in studying the motion of bubbles flowing through nozzles.

A mathematical model was set up to predict the bubble motion. The various forces included in the model are the drag force, the apparent mass force, the buoyancy force, the bubble expansion force and the history forces.

Comparisons between experiments and theories were made through a "point-to-point" numerical testing procedure. Results show that the bubble trajectory can be reasonably predicted (within 10% accuracy) by an equation of motion which includes a suitable drag force (dependent on relative velocity) and an apparent mass force (proportional to relative acceleration). Suggestions regarding the further improvement of the theory are also made.

Key Words: bubble trajectory, nozzle, drag force, apparent mass force

1. INTRODUCTION

Flow systems involving a mixture of gas and liquid have many applications in chemical engineering and power generation processes. A special case is the flowing of dispersed gas bubbles in a liquid stream. It is an area of fundamental interest in the study of two-phase flow. One of the basic issues in mathematical modeling of two-phase flow system is to correctly formulate the momentum and energy interactions between two phases. In steady flow of gas bubbles in a liquid, the momentum interaction is often expressed by a drag force which is a function of bubble sizes, shapes and the relative velocities between the gas bubbles and the liquid flow. When there is unsteady relative motion, additional forces due to the apparent mass effect and viscous momentum diffusion are included. Usually, evaluation of these forces relies on experimental correlations or theories which are developed from special situations where only a single effect is dominant, such as single bubbles rising steadily in stagnant liquid or a sphere accelerating in an ideal flow. In a flow situation where all the effects are present, separate evaluation of the individual effects is often difficult, if not impossible.

This paper presents the results of an experimental study on a well-defined bubbly flow where only the drag force and the apparent mass force are expected to be significant. The chosen subject is the flow of individual air bubbles in water through nozzles in a range of liquid flow rates. The bubble sizes range from 0.15 to 0.4 cm dia. Many effects such as wall friction, phase change and heat transfer are expected to be negligible.

The experiments produced bubble trajectory data which provided the basis for evaluating the existing correlations for the drag coefficient, C_d, and the apparent mass force are evaluated and discussed in light of the comparisons with the experiments.

†Present address: Department of Mechanical Engineering, National Taiwan University, Taipei, Taiwan 10764, R.O.C.

2. THEORY

2.1. Equations of motion

In dealing with the motion of a single bubble, small compared with the nozzle dimensions, it is reasonable to assume that the average liquid motion is unaffected by the bubble. The equation of motion for a bubble moving in a liquid in vertical direction, z can be written as

$$\rho_G v_G \frac{dv_G}{dz} = -\frac{dp}{dz} - \rho_G g - f_{LG}. \quad [1]$$

Here ρ_G is the bubble density and v_G its velocity; p is the liquid pressure. The term f_{LG} represents the interaction between the gas bubble and the liquid. For the liquid flow, the equation of motion is

$$\rho_L v_L \frac{dv_L}{dz} = -\frac{dp}{dz} - \rho_L g, \quad [2]$$

where ρ_L is the liquid velocity and v_L its average velocity. Combining [1] and [2], the equation of motion for the bubble becomes

$$\rho_G v_G \frac{dv_G}{dz} = \rho_L v_L \frac{dv_L}{dz} + (\rho_L - \rho_G)g - f_{LG}. \quad [3]$$

In the development of a general two-phase flow theory, f_{LG} is the sort of term which often requires empirical correlations to give a solution. For motion of a bubble in a fluid, this term can be made up of several components, each of which represents a separate effect. Possible components are as follows:

(*1*) *A drag force,*

$$f_d = \tfrac{3}{4} C_d \frac{\rho_L}{d} (v_G - v_L)|v_G - v_L|, \quad [4]$$

where C_d is a drag coefficient, d is the bubble diameter. C_d is dependent on the Reynolds number (based on relative velocity) and the bubble shape.

(*2*) *An apparent mass force,*

$$f_a = C_a \rho_L \left[\frac{\partial}{\partial t} (v_G - v_L) + v' \frac{\partial}{\partial z} (v_G - v_L) \right], \quad [5a]$$

which accounts for the kinetic energy change associated with the liquid motion induced by the bubble. v' is a characteristic convective velocity of the induced liquid flow. Choices of v' result in different forms of the apparent mass force. For example, Murray (1965) chose $v' = v_G - v_L$. Soo (1967) and Wallis (1969), arguing that the induced circulation is convected with the bubble, chose $v' = v_G$. Lahey (1977) suggested the convective part of this force as

$$f_a = C_a \rho_L \left(v_G \frac{\partial v_G}{\partial z} + v_L \frac{\partial v_L}{\partial z} - 2 v_G \frac{\partial v_L}{\partial z} \right), \quad [5b]\dagger$$

such that it is invariant under coordinate transformation.

The formulation of the apparent mass force depends also on the flow field. Yeh & Yang (1968) studied the motion of a spherical bubble in a source or sink flow. In their analysis, the convective apparent mass force can be identified as

$$f_a = \tfrac{1}{3} \rho_L v_G \frac{dv_G}{dr} - \left(\frac{d}{2r} \right)^2 \rho_L v_L \frac{dv_L}{dr}, \quad [5c]$$

where d is the bubble diameter and r its displacement. This shows that the apparent mass force, probably, can not be universally represented by the form [5a].

†Recent work by Drew & Lahey (1987), gives the apparent mass term as

$$f_a = C_a \rho_L \left(v_G \frac{dv_G}{dz} - v_L \frac{dv_L}{dz} \right).$$

(3) An effect of rate of change of bubble volume in the pressure field,

$$f_e = \tfrac{3}{8} C_s \frac{\rho_L}{d} (v_G - v_L) v_G \frac{d(d)}{dz}. \quad [6]$$

For a spherical bubble in uniform potential flow $C_s = 4$. Yeh & Yang (1968) showed that for a bubble moving in a source or sink flow $C_s = 2.67$. This force is similar in nature to the apparent mass force.

(4) A momentum diffusion force representing the history of the viscous flow field near the bubble surface. Basset (1961) obtained an expression of this effect for a solid sphere in laminar flows:

$$f_b = C_h \frac{3}{2} \left(\frac{\rho_L \mu_L}{\pi d^2} \right)^{1/2} \int_{t_0}^{t} \frac{\frac{d}{d\tau}(v_G - v_L)}{(t-\tau)^{1/2}} d\tau; \quad [7]$$

μ_L is the liquid viscosity. The time derivative is taken with respect to a coordinate system moving with the bubble. For a small bubble $C_h = 4$, according to Morrison & Steward (1976).

(5) Morrison & Steward (1976) found an additional momentum diffusion term for a small bubble. It was written as

$$f_m = \frac{d}{12(\pi \nu_L)^{1/2}} \int_{t_0}^{t} \frac{\frac{d^2}{d\tau^2}(v_G - 3v_L)}{(t-\tau)^{1/2}} d\tau. \quad [8]$$

Here ν_L is the liquid kinematic viscosity. This term appears in the equation of motion of a spherical bubble in an accelerating liquid at low Reynolds number (in the creeping flow range).

So far we have presented a general survey of the existing theories on the various forces acting on the bubble. Since the flows with which we are concerned are turbulent, bubbles are not spheres, there is slip and boundary layer separation at the bubble surface, and the bubbles do not move in straight lines, none of these expressions can be known *a priori.* Before we have any further knowledge on these forces, we propose to combine various forces on the bubble linearly to form the equation of motion for the bubble, and to study its mathematical consequences by varing the various force coefficients.

2.2. Evaluation of the force coefficients

Usually, the drag coefficient is estimated from correlations of bubble rise speed in a large extent of liquid. Wallis (1974) presented a universal correlation scheme to correlate the bubble rising speeds as a function of bubble size. This correlation is presented in terms of dimensionless bubble velocity v^* and dimensionless diameter d^* with

$$P \equiv \frac{\sigma^3 \rho_L^2}{\mu_L^4 g(\rho_L - \rho_G)}$$

as a parameter, where σ is the surface tension; v^* and d^* are defined as

$$v^* = v_\infty \left[\frac{\rho_L^2}{\mu_L g(\rho_L - \rho_G)} \right]^{1/3} = \left(\frac{4}{3} \frac{\mathrm{Re}_\infty}{C_{d\infty}} \right)^{1/3} \quad [9]$$

and

$$d^* = d \left[\frac{\rho_L g(\rho_L - \rho_G)}{\mu_L^2} \right]^{1/3} = (\tfrac{3}{4} C_{d\infty} \mathrm{Re}_\infty^2)^{1/3}, \quad [10]$$

where v_∞ is the bubble rise speed in an infinite medium. $C_{d\infty}$ is the drag coefficient of a bubble rising in a large pool of stagnant liquid, defined as

$$C_{d\infty} = \frac{4}{3} \frac{dg(\rho_L - \rho_G)}{\rho_L v_\infty^2}; \quad [11]$$

Table 1. Bubble rise speed and drag correlations

Region	Bubble rise speed correlation[a]	Drag correlation	Range
1	$v^* = \frac{1}{3}r^{*2}$	$C_d = \frac{16}{Re}$	$Re < 0.49$
2	$v^* = 0.307r^{*1.21}$	$C_d = \frac{20.68}{Re^{0.643}}$	$0.49 < Re < 33$
2D	$v^* = \frac{2}{27}r^{*2}$	$C_d = \frac{72}{Re}$	$Re > 33$
3	$v^* = \sqrt{2}r^{*-1/2}P^{1/6}$	$C_d = \frac{Re^4}{48P}$	$We = 4$
4	$v^* = \sqrt{2}P^{1/12}$	$C_d = \frac{0.47Re}{P^{1/4}}$	$We < 8$
5	$v^* = r^{*1/2}$	$C_d = \frac{8}{3}$	

[a] $r^* = \frac{1}{2}d^*$.

Re_∞ is the Reynolds number, defined as

$$Re_\infty = \frac{\rho_L v_\infty d}{\mu_L}. \quad [12]$$

The correlation for terminal speed of a rising bubble gives $C_{d\infty}$ as a function of Re_∞ with P as a parameter. Table 1 shows various regions of bubble behavior and the coresponding drag correlation. Here the subscript ∞ is dropped for simplicity.

In general, when bubbles are moving in a liquid the drag force may not be balanced with gravity. For example, with bubbles moving in an accelerating or decelerating liquid flow field, the liquid inertia force may become the balancing force for the drag force and some other forces mentioned earlier. Thus it is desirable to correlate the drag coefficient with Re and the Weber number, We. Here, Re and We are based on the relative velocity $v_G - v_L$, and are defined as

$$Re = \frac{\rho_L(v_G - v_L)d}{\mu_L} \quad [13]$$

and

$$We = \frac{\rho_L(v_G - v_L)^2 d}{\sigma}. \quad [14]$$

The force balance for the bubble rising steadily relative to a liquid under gravity can be rewritten in terms of Re and We as

$$C_d = \frac{4}{3}\cdot\frac{Re^4}{We^3 P}. \quad [15]$$

Eliminating P between [15] and table 1 gives table 2a, where C_d is a function of Re and We. When bubbles are spherical, C_d is a function of Re only; when bubbles become very distorted C_d is a function of We only. In region 3, We = const (around 4) and C_d is not explicitly available. Physically, in this region the bubbles adjust their shapes to keep We = const. For bubbles and fluid drops, We in region 3, according to different investigators (Wallis 1974) falls in the range $3.6 < We < 4$. The drag coefficient presented in table 2a is recommended for bubbles moving in clean water (filtered or distilled water).

Table 2b gives the drag correlation for bubbles rising in tap water. In tap water, the drag correlation in region 2D is closely represented by the solid particle drag correlation,

$$C_d = \frac{6.3}{Re^{0.385}} \quad \text{for} \quad Re > 100,$$

and is identified as region 2B. Region 3 is absent for bubbles rising in "dirty" water. Apparently

Table 2a. Bubble drag correlations (clean water)

Region	Drag correlation	Range
1	$C_d = \frac{16}{Re}$	$Re < 0.49$
2	$C_d = \frac{20.68}{Re^{0.643}}$	$0.49 < Re < 33$
2D	$C_d = \frac{72}{Re}$	$Re > 33$; $We < 4$
3	$We = 4$	
4	$C_d = \frac{We}{3}$	$We < 8$
5	$C_d = \frac{8}{3}$	

Table 2b. Bubble drag correlations (tap water)

Region	Drag correlation	Range
1	$C_d = \frac{16}{Re}$	$Re < 0.49$
2	$C_d = \frac{20.68}{Re^{0.643}}$	$0.49 < Re < 100$
2B	$C_d = \frac{6.3}{Re^{0.385}}$	$100 < Re$
4	$C_d = \frac{We}{3}$	$Re > \frac{2065.1}{We^{2.6}}$
5	$C_d = \frac{8}{3}$	$We > 8$

the surface cleanness of the bubble has a significant effect on the boundary layer flow around the bubble. Figure 1 gives the overall picture of the drag correlation for bubbles rising in water.

There are many factors which may cause the steady-state drag correlation to differ from the drag correlation in an accelerating or decelerating flow situation. For example, in a transient pressure field the boundary layer structure may be different from that of a steady-state pressure field at comparable Re, due to the limitation of the time scale of viscous momentum diffusion. The turbulence in the surrounding field, which may be small compared with the mean flow, may be significant in comparison with the relative velocity between the air bubble and the water. The oscillation in bubble shape excited by the liquid pressure change will also affect the drag force.

Torobin & Gauvin (1961) measured the drag coefficients of single spheres in steady accelerated motion in turbulent flow. Their results showed that the drag coefficient can be greater or smaller than the steady-state value, depending upon the intensity of turbulence and Re. Herringe (1976) showed that the theory based on steady flow drag did not adequately predict the mean fall velocities of small spheres falling through vertically oscillated liquids. Studies on motion of spheres (Tyler & Salt 1977) and droplets (Temkin & Kim 1980) induced by shock waves also showed drag

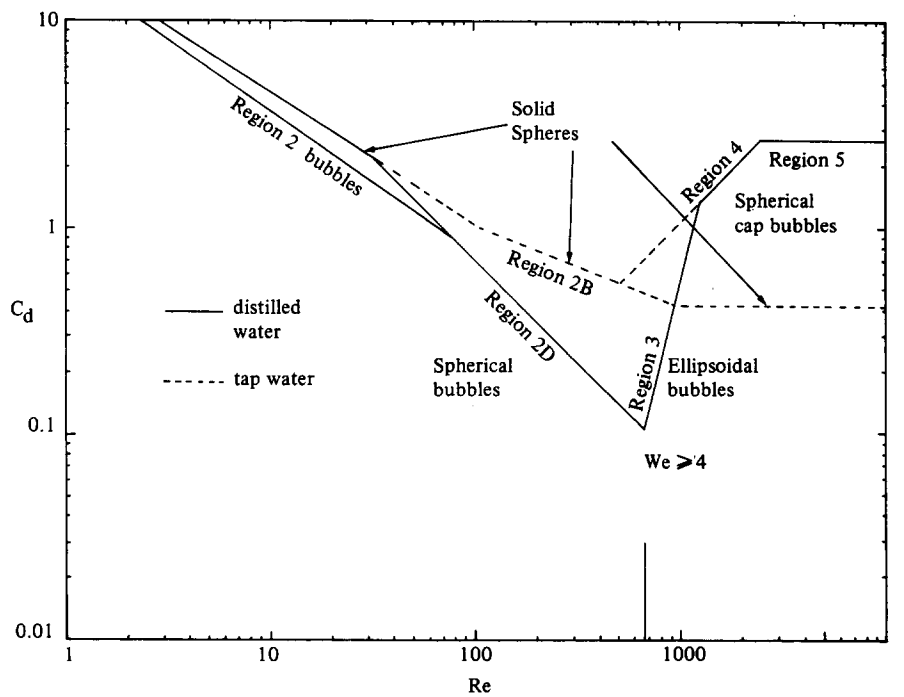

Figure 1. Drag correlation of air bubbles rising in water.

coefficient values which are larger than the steady-state values at the same Re. For bubbles we expect similar things may happen, although they may arise for different reasons.

The apparent mass force coefficient for a solid sphere accelerating in a uniform potential flow is found to be 0.5. Theoretically, the apparent mass coefficient is a constant tensor for a rigid body (Batchelor 1967) which depends upon the actual shape of the body. For an oblated ellipsoid with an axis ratio of 2, C_a is found to be 1.12 in a uniform potential flow (Lam 1972). For a bubble, C_a will vary as it adjusts its shape to conform with the liquid pressure outside the bubble. In the real situation, when vortex shedding or flow separation occurs, C_a will presumably be greater than the value given by the potential flow theory, because in such cases more liquid motion is involved.

3. EXPERIMENTAL APPARATUS AND MEASUREMENTS

3.1. Apparatus

The schematic diagram of the water flow system is shown in figure 2, which consists of a Plexiglas water channel, a suction pump and a water feed tank. Figure 3 shows the dimensions of the Plexiglas channel. The inlet section of the Plexiglas channel is a rectangular box (61 cm high × 15.24 cm^2) filled with fibrous materials to redistribute the incoming water jet and subdue vortices. The main test section is a 183 cm long water channel with a rectangular cross section 15.24 × 5.08 cm. The nozzles are formed by inserting Plexiglas blocks of varying shapes to create the desired accelerating and decelerating flows. Figure 4 shows the dimensions of the nozzles.

3.2. Bubble generating system

Bubbles were introduced into the flow system through a 0.11 cm i.d. stainless steel tube which was bent along the flow direction near the nozzle entrance. Air was supplied by a plastic syringe connected to the bubble generating tube. The movement of the syringe piston was controlled by

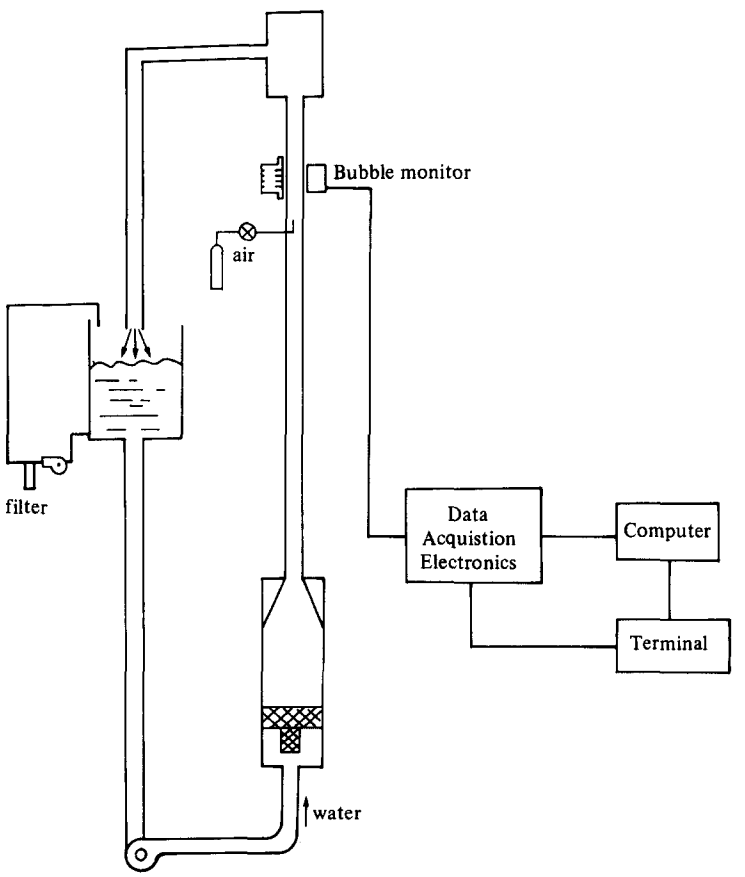

Figure 2. Experimental apparatus.

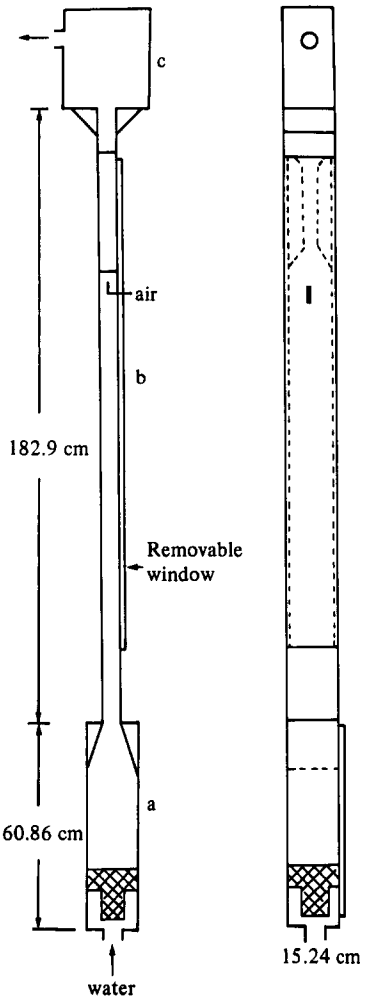

Figure 3. Water channel.

a screw. The syringe was filled with water. A second syringe was used to inject a small amount of air into the primary syringe. The arrangement enabled us to generate one air bubble at a time with water speeds up to 60 cm/s. For higher flow rates, a short piece of a larger tube (0.63 cm o.d. × 0.56 cm i.d. × 2 cm long) was mounted on the tip of the stainless steel tube. When a bubble was released from the small tube, it rose to the exit of the large tube and became trapped by the wake behind (figure 5). The bubble would remain hovering near the opening of the large tube until a squirt of water from the syringe released it. The bubbles generated by the small tube were in the range 0.15–0.25 cm, depending upon the flow rates. Larger bubbles, around 0.4 cm dia, were generated with the large tube attachment. The bubble sizes were determined from photographs. The bubble shape was very close to spherical near the tube opening. As the bubbles flowed through the nozzle, the bubble shape would vary to conform with the surrounding water pressure. A spherical bubble tended to become ellipsoidal near the throat (with the major axis across the flow direction).

3.3. Bubble motion detector

Bubble motion through the nozzles was monitored with stacked arrays of phototransistors. The phototransistor bubble detector worked on the principle of interruption of a light beam by a bubble passing between a sheet of light and a row of phototransistors. The bubble position along the nozzle was determined by its crossing through the light path to several rows of phototransistors. When a bubble was detected, the horizontal position across the width of the channel as well as the elapsed time since the previous stage were noted. Eighteen stages (1 cm apart) of phototransistor arrays were set up to cover a major portion of the converging and diverging sections of the nozzle. The

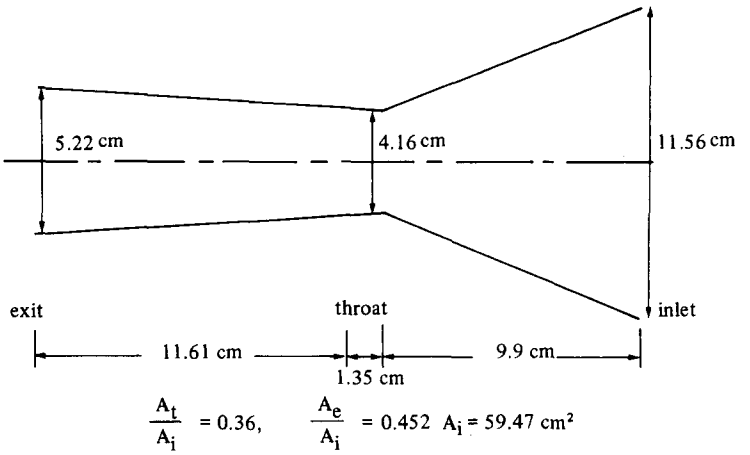

Nozzle No. 1

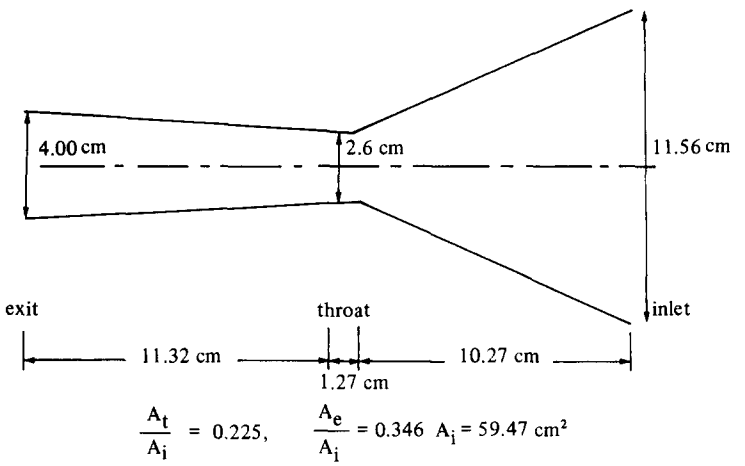

Nozzle No. 2

Figure 4. Nozzles Nos 1 and 2.

Figure 5. A bubble trapped by the flow wake.

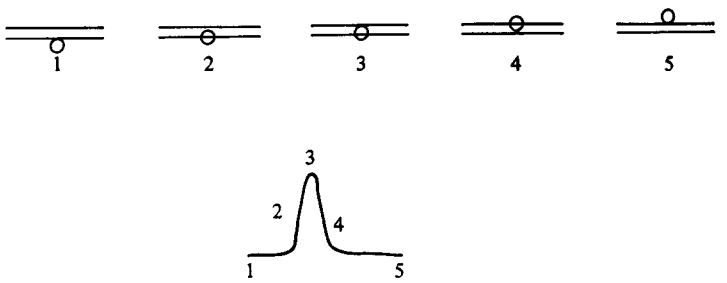

a. The bubble signal and the corresponding bubble positions.

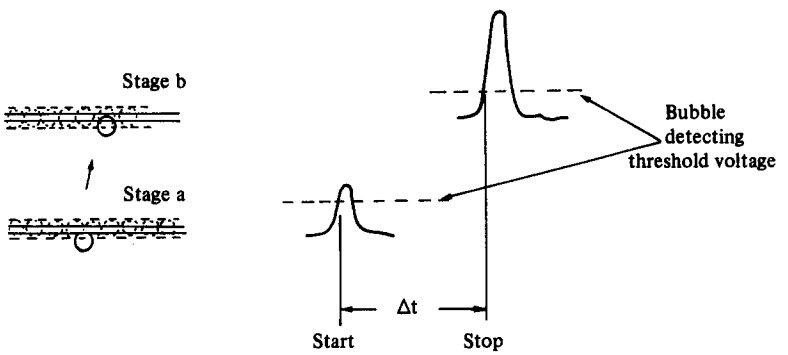

b. The measurement of Δt for the bubble to travel from stage a to stage b.

Figure 6. The bubble signal.

bubble detector provided specific data of the bubble motion through the nozzle, its position as well as its velocity.

3.4. Measurements and error analysis

The accuracy of the bubble motion detector in measuring bubble position and traveling time may be subject to various kinds of errors. Figure 6 shows a bubble crossing a detecting station window slit and its signal as well as the time measurement between two adjacent slits. The width of the slit is 0.1 cm. The uncertainty in the bubble vertical position should be within $+0.05$ cm.

Although the bubbles were released at the center of the flow channel, they might wander off the centerline due to turbulence and nonuniformity in flow distribution. Photographs taken with a stroboscope in darkness showed that single bubble trajectories were mostly straight lines. These might not coincide with or be exactly parallel to the centerline, but they generally stayed within an area of 1 cm^2 around the centerline. Considering the uncertainties in bubble position and traveling time measurements, the uncertainty in bubble velocity measurement is within $\pm 5\%$.

The performance of the bubble detector was tested by recording the displacement history of a free-falling steel ball in air. The measured velocities (in the comparable range of bubble experiments) were within 2–6% of the theoretical predictions. The acceleration deduced from the steel ball displacement data was $9.8\ m/s^2 \pm 5\%$. A second check on the accuracy of the optical measurement system was to measure the rise speed of a bubble in stagnant water. For a 0.4 cm dia bubble, the rise speed measured by the optical bubble detector was comparable with the data deduced from the photographs of the bubble trajectories taken with a stroboscope. The measured rise speed was 20 cm/s, while according to the steady-state drag correlation the calculated rise speed was 23 cm/s.

Water velocities were measured using a $\frac{1}{16}''$ Pitot tube. The measurements were consistent with the flow rate measurements within 4%. Near the nozzle entrance, the average water velocity based on the flow rate measurement was about 90–95% of the centerline velocity. The velocities within a 4 cm^2 area around the centerline were uniform within 3%. Water velocities along the nozzle

centerline were obtained by moving the Pitot tube each time to a new position while maintaining the overall flow rate constant. Thus, the water velocity measurements were subjected to the uncertainty due to flow rate control. The overall uncertainty in the liquid velocity measurement, including the effects of turbulence, manometer fluid surface tension and random experimental errors, was estimated to be within $\pm 5\%$.

4. DATA ANALYSIS

In total, six different experiments were conducted to investigate the bubble motion in two different nozzles. Table 3 lists the test conditions for the six sets of experiments. In particular, test 6 was performed with bubbles flowing downward. For each test condition, a large number (ranging from 30 to 46 repeated runs) of bubble trajectories were recorded. Figures 7–12 show typical bubble vertical displacement histories. Figures 13–18 show the statistically averaged bubble velocities along the nozzle centerline. The error bars indicate the statistical variance of the measurements.

The bubble trajectory data were subject to variations in bubble size and the fluctuations of bubble and liquid velocities. At high liquid flow rates (figures 7, 8 and 10), the theory is insensitive to even a 50% variation in bubble size. At low flow rates, the influence of bubble size variation is more pronounced; although as a percentage it is relatively small, a size variation of 20% produces a difference of $\pm 2.5\%$ in bubble traveling time.

The theoretical calculation is not very sensitive to the assumed bubble initial velocity. The influence of the bubble initial velocity is only evident in the first 3 cm of the numerical integration. The theory is more sensitive to the changes in liquid velocities. A $\pm 5\%$ variation in the liquid velocity could vary the bubble traveling time up to $\pm 5\%$. Since the theory is relatively insensitive to the variations of bubble size and initial velocity any significant discrepancies between the test data and the theory would be an indication of the inadequacy of the theory on various force coefficients. Considering only the drag force and the apparent mass force, the equation of bubble motion [3] was integrated numerically to produce the bubble velocities as well as the position at different times in the nozzle. Here $v' = v_G$ for [5a] was used in the calculation.

The drag coefficient correlation was the one for tap water. Figures 7–12 show the comparison of theory and experiments on the bubble displacements history. Figures 13–18 present the measured and predicted bubble velocities. In general the theory does not look too bad, except against the data of tests 3 and 6.

Comparison of the theory with the data of test 3 indicates that the forces predicted by the theory should be reduced in order to fit the data, where as the data of test 6 showed that the theory underpredicts the forces on the bubble. Since in tests 3 and 6, the theory showed that the apparent mass force is relatively unimportant, it is the drag correlation which is primarily responsible for the discrepancy between the theory and the data. In tests 3 and 6, the bubbles were generally moving in the Re range where vortex shedding would occur in the steady-state situation. If, during acceleration or deceleration vortex shedding is suppressed due to lack of time to develop, the

Table 3. Water velocities in the nozzle

			Water velocity (m/s)								
			Converging section ($-11.5\,\text{cm} < z < 0.5\,\text{cm}$)			Throat ($0.5\,\text{cm} < z < 1\,\text{cm}$)			Diverging section ($1\,\text{cm} < z < 8.5\,\text{cm}$)		
Test	Nozzle	Flow rate $\times 10^{-3}$ (m^3/s)	-11.5	-7.5	-5.5	-3.5	-1.5	0.5	2.5	6.5	8.5
1	1	4.92 (up flow)	0.89	1.12	1.38	1.72	2.12	2.42	2.27	2.16	2.10
2	1	4.0 (up flow)	0.70	0.96	1.09	1.43	1.72	1.98	1.85	1.82	1.73
3	1	2.8 (up flow)	0.50	0.63	0.76	0.96	1.22	1.36	1.33	1.29	1.24
4	2	4.0 (up flow)	0.83	1.04	1.26	—	2.33	3.00	2.82	2.53	2.43
5	2	4.92 (up flow)	1.01	1.28	1.54	—	2.86	3.65	3.45	3.08	2.95
6	2	2.8 (down flow)	0.59	0.72	0.87	—	1.73	2.18	2.02	1.84	1.75

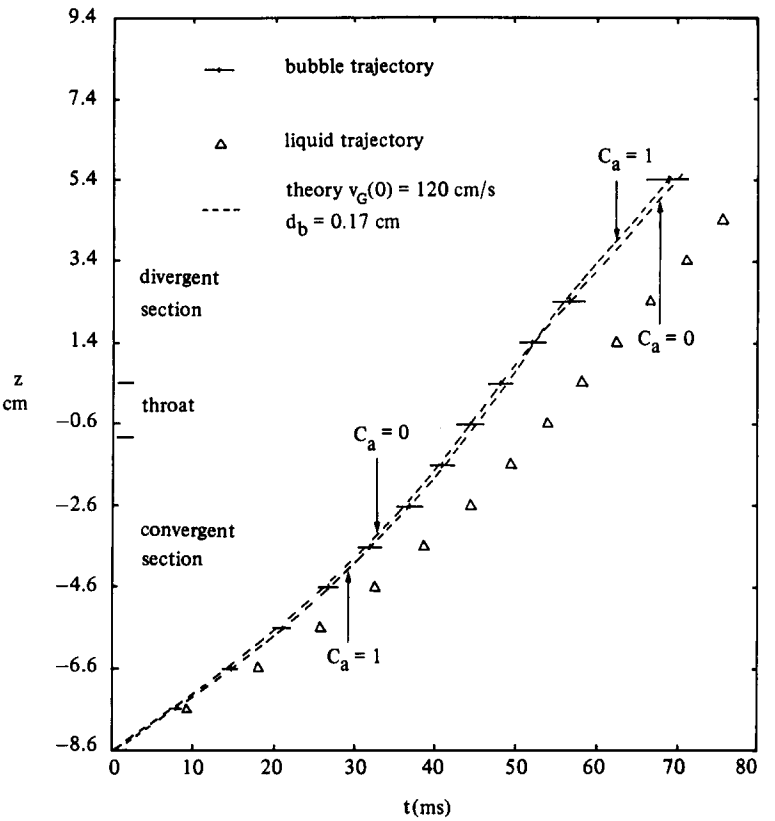

Figure 7. Bubble vertical displacement vs time in nozzle No. 1 (test 1).

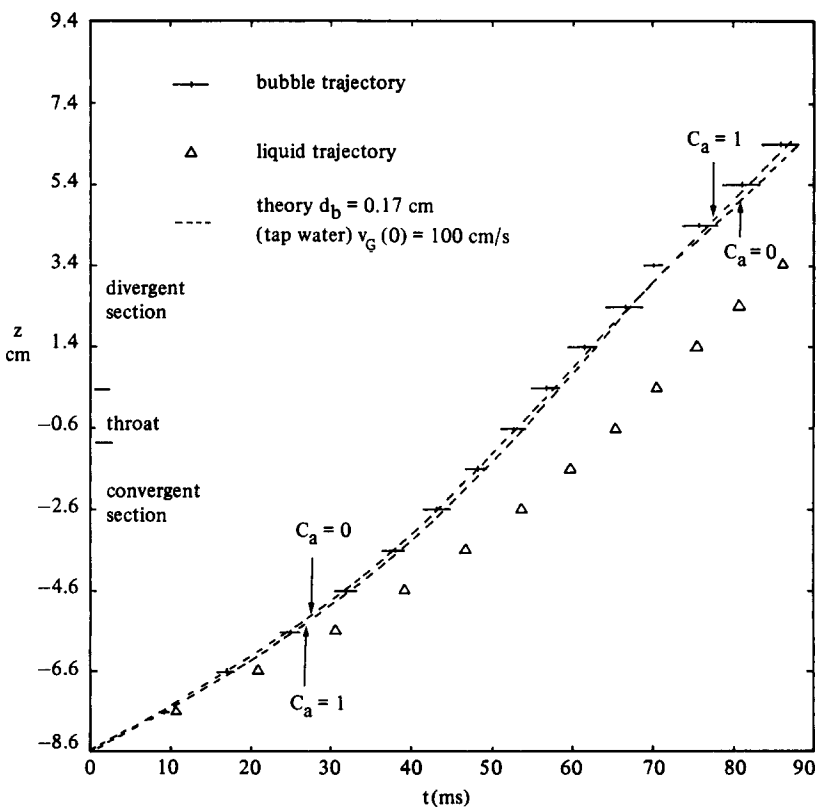

Figure 8. Bubble vertical displacement vs time in nozzle No. 1 (test 2).

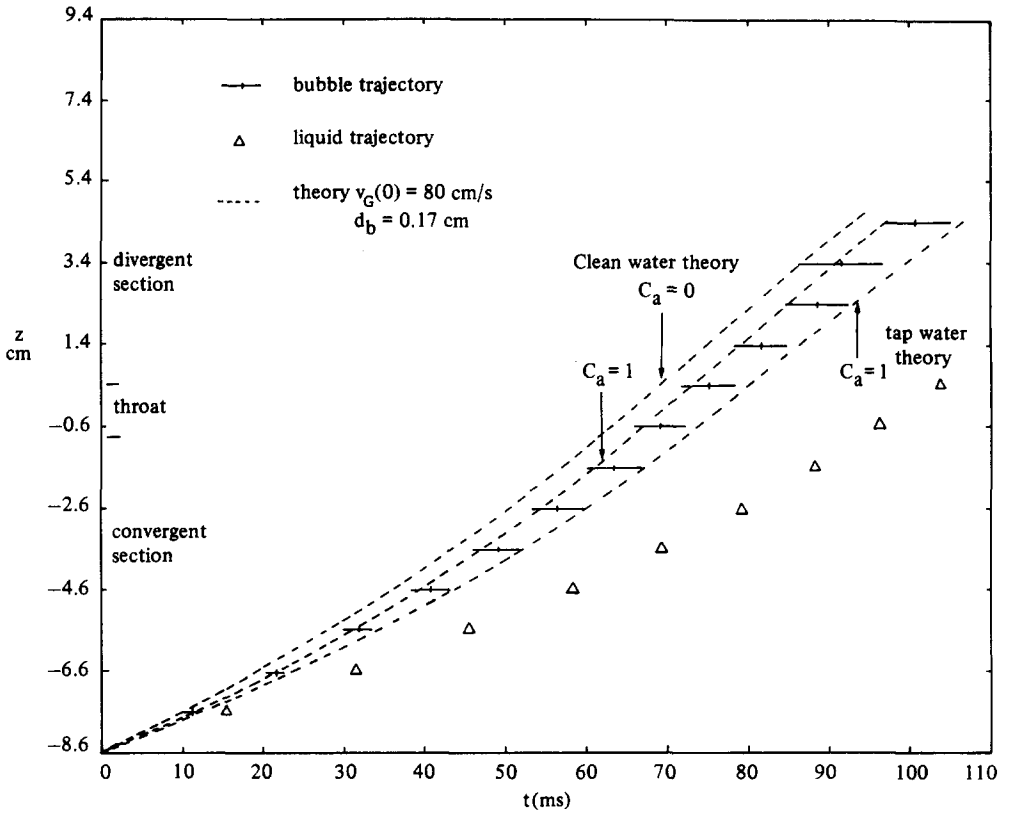

Figure 9. Bubble vertical displacement vs time in nozzle No. 1 (test 3).

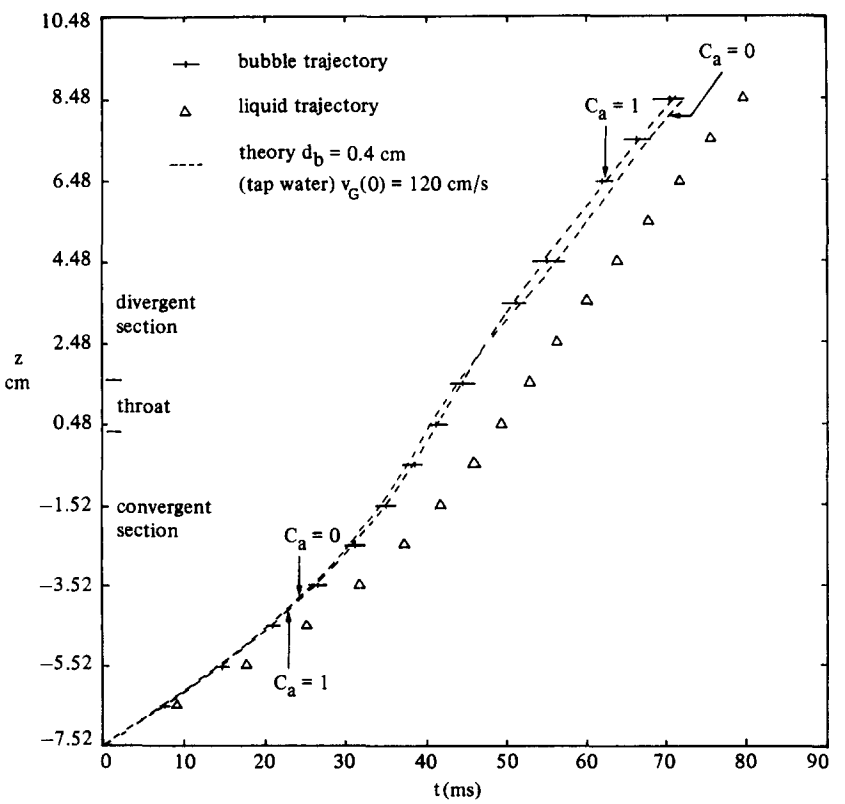

Figure 10. Bubble vertical displacement vs time in nozzle No. 1 (test 4).

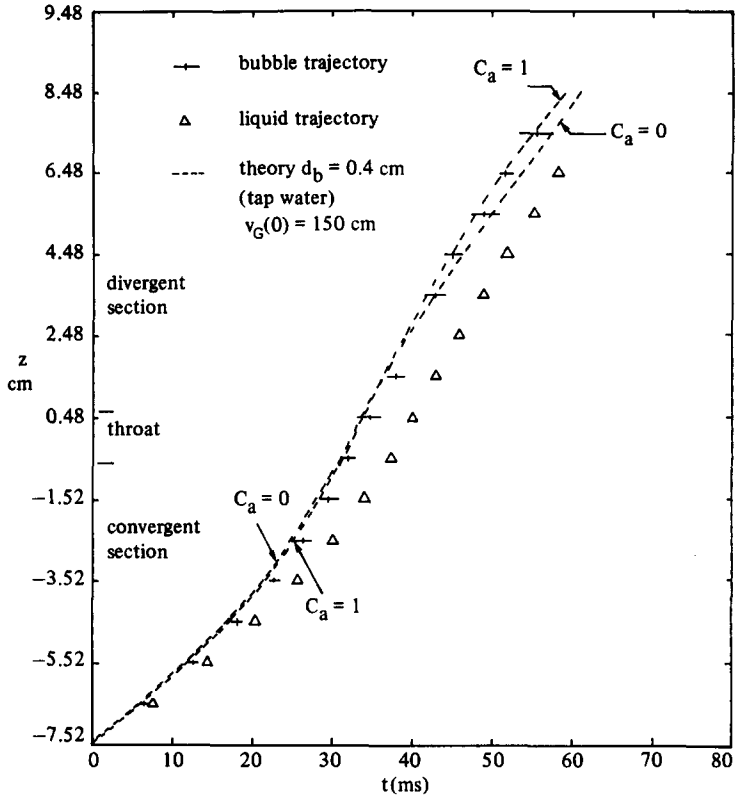

Figure 11. Bubble vertical displacement vs time in nozzle No. 1 (test 5).

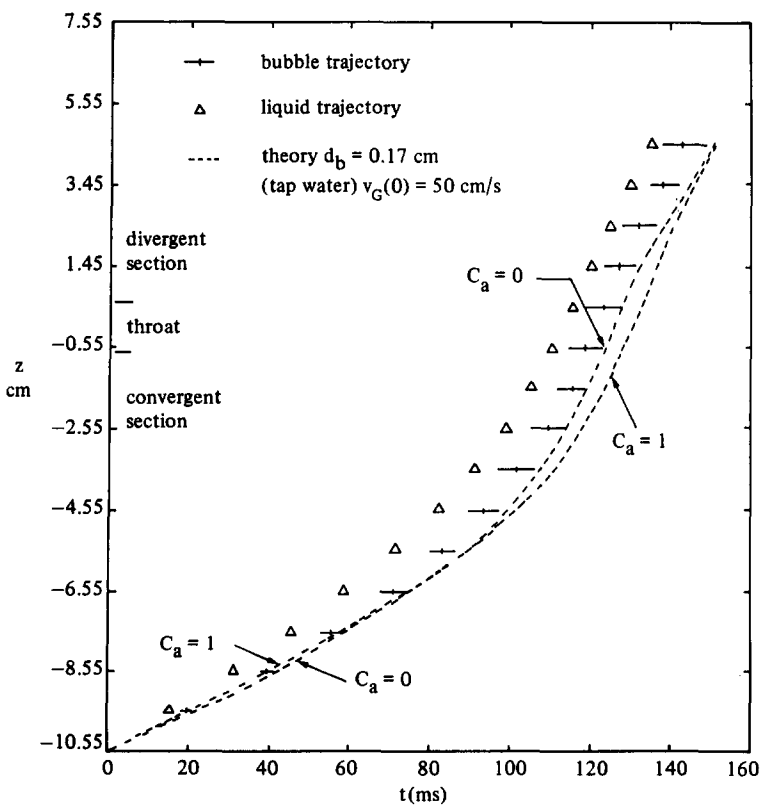

Figure 12. Bubble vertical displacement vs time in nozzle No. 1 (test 6).

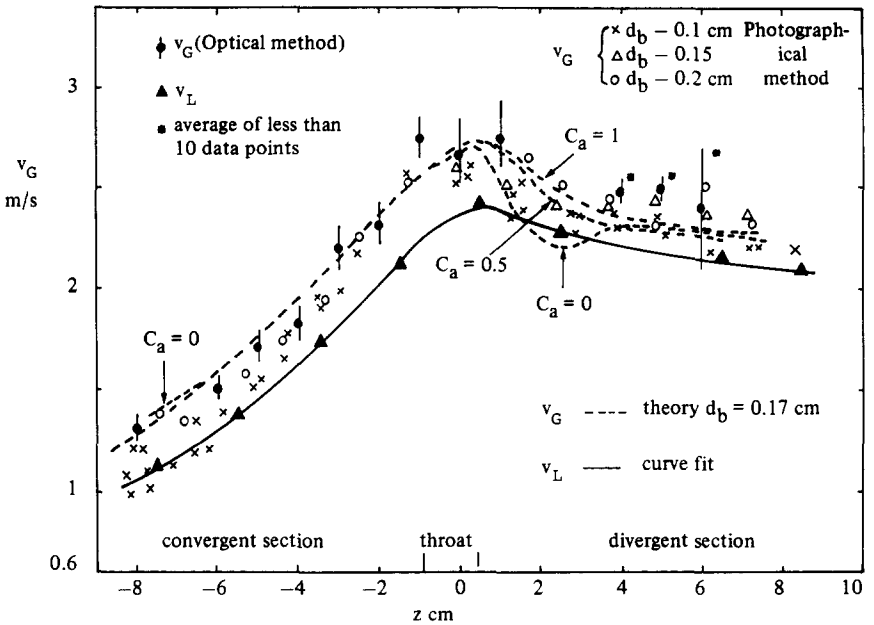

Figure 13. Vertical bubble velocity along the centerline of nozzle No. 1 (test 1).

unsteady-state drag will be less than the steady-state value. Additional test results using a steel ball ($d = 0.2$ cm) under test 1 condition, suggested that the drag force should be 25–75% higher than the steady-state value. For a closer examination of the data in comparison with the theory, a numerical comparison procedure was adopted, which calculates the sum of squares of the differences between the data and the theory. The theory was made to fit the data by adjusting the steady-state drag coefficient with an arbitrary multiplier N and varying the apparent mass coefficient from 0 up to 5. The results of the numerical comparison indicated that for each test data there is a combination of C_a and N that would give the best agreement between theory and experiment. For each test condition, the values of C_a and N, which give the best fit, scatter over a significant range. The C_a-values are mostly in the range 0.5–3. As for the drag coefficients the best N-values cover the range 0.2–3. The wide variations in C_a and N partially reflect the fluctuations of the experimental conditions. While this sort of numerical comparison does not narrow down

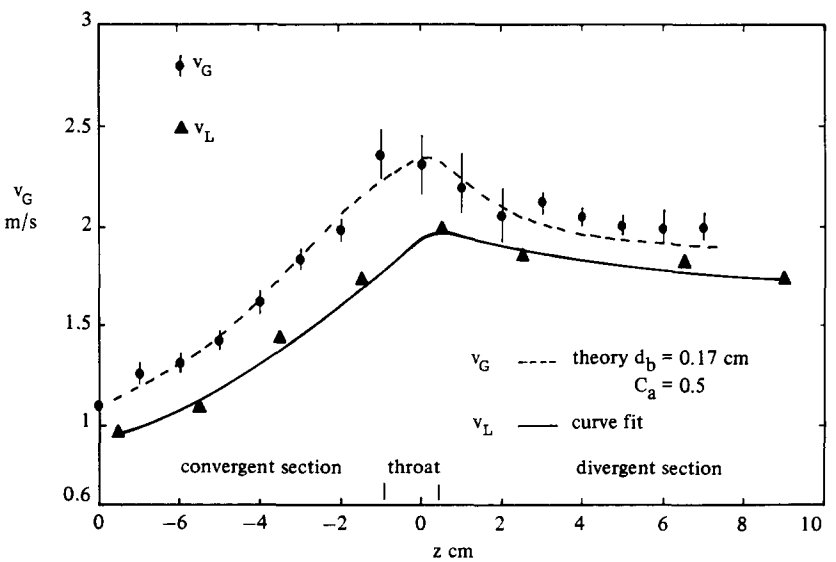

Figure 14. Vertical bubble velocity along the centerline of nozzle No. 1 (test 2).

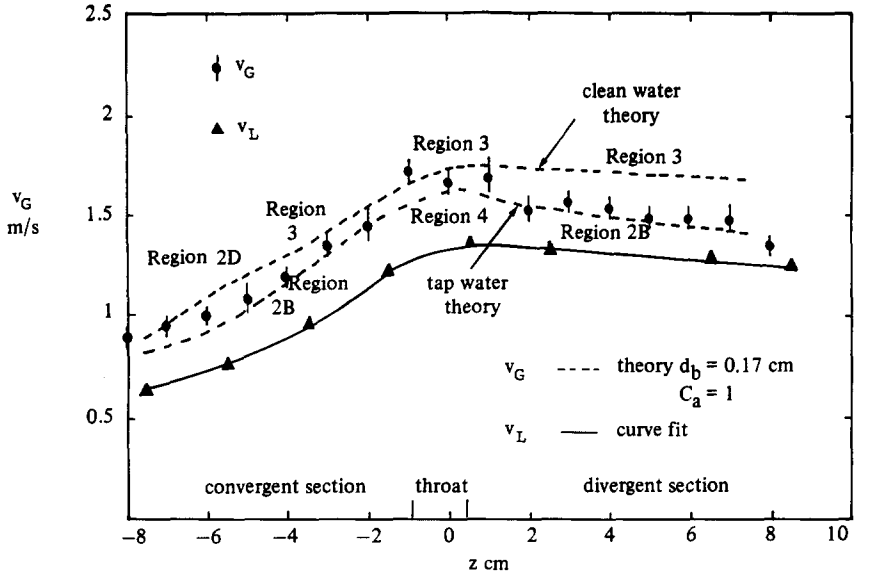

Figure 15. Vertical bubble velocity along the centerline of nozzle No. 1 (test 3).

the specific values of C_a and N, the range of the values are not physically unrealistic, considering the facts that bubbles are not spherical, there is oscillation in bubble shape and the flow is turbulent.

Since the bubbles were observed to change their shapes as they moved through the nozzle, one would expect that both the main flow streamlines relative to the bubble and the boundary layer structures of the flow around the bubble would be affected by the bubble oscillation. The oscillation in bubble shape will affect the drag force and the apparent mass force and introduce additional "forces". There is evidence indicating that bubbles change from spherical shape to oblated ellipsoid in the nozzle. The natural frequency of this mode of oscillation for a gas bubble in a nonviscous liquid, as calculated by Lamb (1972), is

$$f = \frac{1}{2\pi}\left(\frac{12\sigma}{\rho_f r^3}\right)^{1/2}.$$

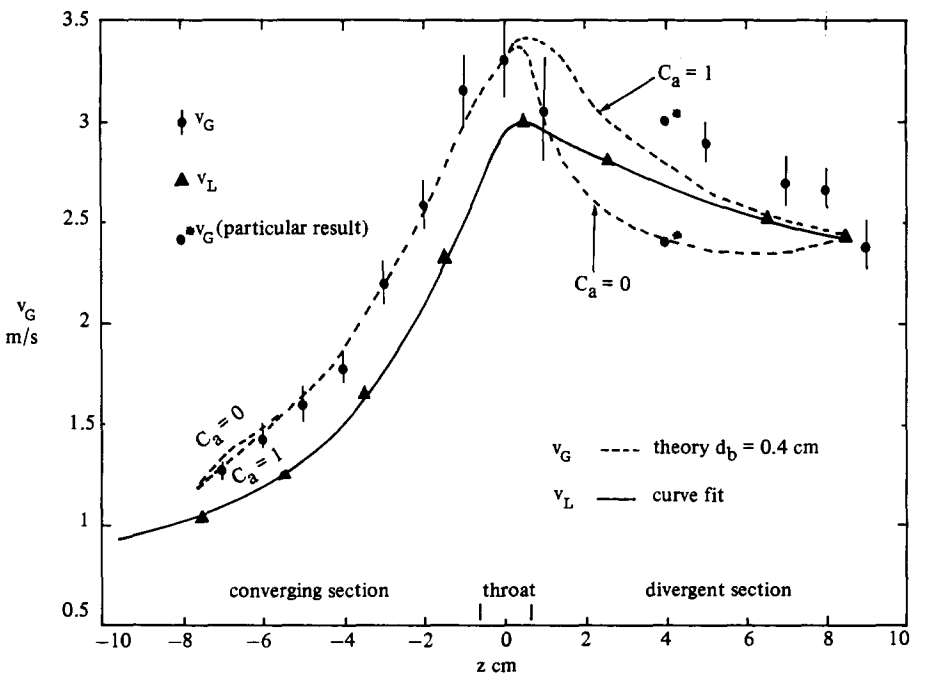

Figure 16. Vertical bubble velocity along the centerline of nozzle No. 1 (test 4).

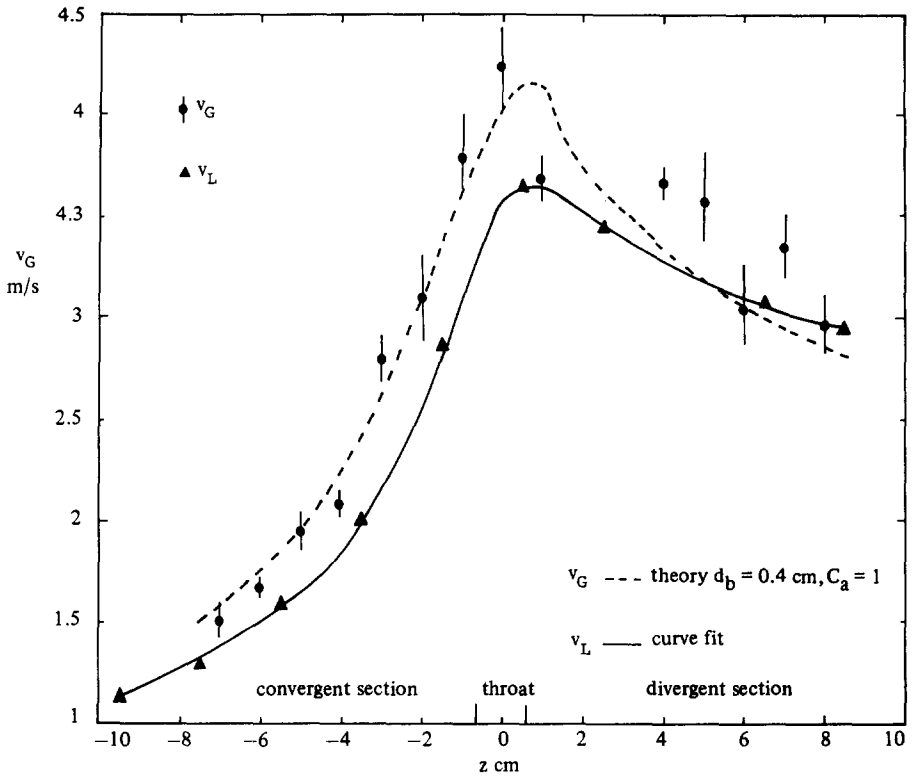

Figure 17. Vertical bubble velocity along the centerline of nozzle No. 1 (test 5).

For an air bubble in water, with $r = 0.1$ cm, $f \approx 150$ cycle/s. In the experiment the bubble residence time in the nozzles ranges from 70 to 160 ms. This implies that the bubble may oscillate 10–20 times in the nozzle. For tests 4 and 5, the bubble radius was around 0.18 cm; the frequency of bubble oscillation was about 60 cycle/s. Bubble oscillation is likely to be an important factor in influencing the drag force and the apparent mass force. The assessment of the influence of bubble oscillation on the drag coefficient requires further knowledge of the boundary layer development in response

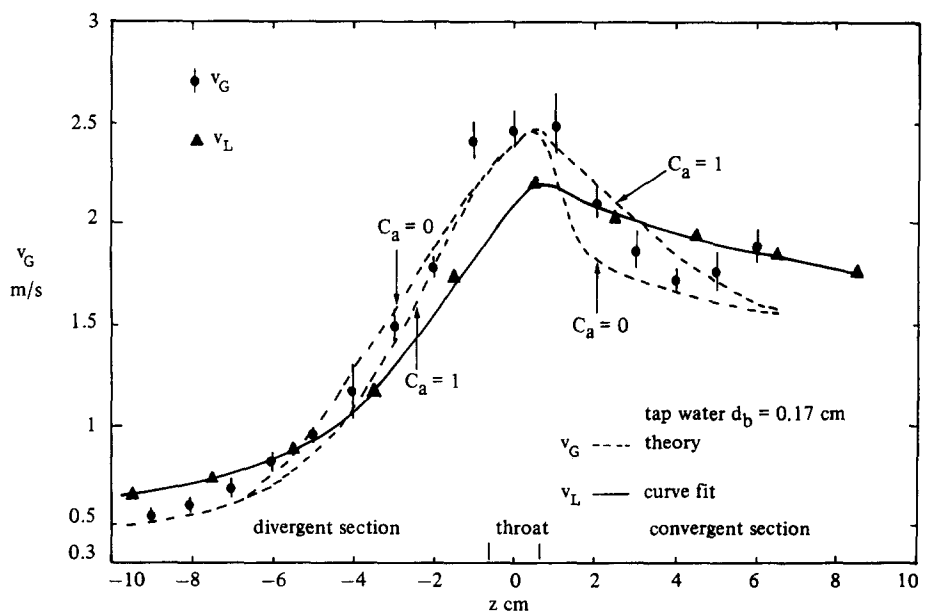

Figure 18. Vertical bubble velocity along the centerline of nozzle No. 1 (test 6).

to the bubble wall oscillation. Bubble oscillation partially explains the deviation of the unsteady-state drag from the steady-state drag.

The effect of bubble shape oscillation on the apparent mass force can be visualized from a simple momentum balance argument. Assuming the apparent mass force is the only force acting on the bubble, we write the force balance in a frame of reference moving at a speed approximately representative of the bubble and the surrounding liquid as

$$f_b = \rho_L \frac{d}{dt}[C_a(v_G - v_L)] = \rho_L C_a \frac{d(v_G - v_L)}{dt} + \rho_L (v_G - v_L) \frac{dC_a}{dt}.$$

This shows that an additional force will arise due to the time variation of C_a. For an order of magnitude estimation of this effect, we assume $v_G - v_L \approx 30$ cm/s and $v_G - v_L$ changes by 10 cm/s and C_a changes from 0.5 to 0.8 in 10 ms. The force due to dC_a/dt is 1.4 times greater than the force due to the relative acceleration. This is equivalent to multiplying C_a by a factor of 2.4 if only the relative acceleration is considered. This numerical estimation shows that C_a-value of 2 or 3 is quite possible if one optimizes the fit between theory and experiment based on a constant value of C_a.

The effects of the momentum diffusion were investigated by numerically integrating the equation of motion and adding [7] and [8]. The results showed that at high flow rates (e.g. test 1 conditions) both effects were not significant, however, the influence of adding the second diffusion term [8] was significant at low flow rates (tests 3 and 6). Considering the time limitation for the diffusion of viscous momentum and the effects of turbulence and boundary layer separation, we would not expect the history forces to be very important. Since the estimation of the history forces is very time-consuming, for practical purpose it would be better to modify the theory by adjusting the drag coefficient and the apparent mass coefficient. Overall, in this work, an equation of motion using the drag correlation for bubbles rising in liquid and an apparent mass coefficient around unity was able to predict the bubble trajectories within 10% accuracy.

The apparent mass force formulation suggested by Lahey (1977) in [5b] is not significantly different from [5a] which we used in the theory. Calculation showed the results using Lahey's apparent mass force give a bubble history curve which only differs within 2% from the curve using [5a]. Use of the apparent mass force expression recently developed by Drew & Lahey (1987) in [3] is not expected to substantially change the conclusions of this work either. The indifference of the theory to different formulations of the apparent mass force reflects that the test conditions selected in this work did not produce strong enough apparent mass forces to distinguish one theory from the other.

According to the present theory the apparent mass force is significantly greater than the drag force only in the vicinity of the nozzle throat. Thus, in order to estimate the apparent mass force, the measurements have to be concentrated in the region ± 2 cm around the throat. The total residence time of the bubble in the region is estimated to be no more than 0.02 s. Accurately tracing the bubble motion in this small region in such a period of time is a difficult task.

5. CONCLUSIONS

1. The trajectory of a single bubble in different nozzles can be represented by an equation of motion which includes a suitable drag force (dependent on relative velocity) and an apparent mass force proportional to the relative acceleration.
2. The drag correlation derived from a bubble rising in a stagnant liquid and an apparent mass coefficient around unity can be used in the theory to predict the bubble trajectory in an accelerating or decelerating flow within 10% accuracy.
3. In acceleration or deceleration, the drag force on the bubble may be different from that in a steady-state situation at comparable Re due to the limitations of the time scale of viscous momentum diffusion, the turbulence in the liquid and the oscillation of the bubble in the liquid and the oscillation in bubble shape. Quantitatively, the unsteady-state drag coefficient may vary $\pm 50\%$ from the steady-state drag coefficient.
4. The apparent mass coefficient is not a constant for bubbles moving in a transient liquid flow field. Numerical estimation shows that a C_a-value of 2 or 3 is quite possible if the fit between theory and experiment is optimized based on a constant value of C_a.

5. The apparent mass phenomenon is three-dimensional in nature and may not be universally represented by a particular form in a one-dimentional approximation.
6. There is no significant quantitative difference between the various formulations of the apparent mass force. One can not discriminate one from the other at this stage.
7. The bubble velocity is distinctly different from that of the liquid. An assumption of homogeneity in velocity for the bubble and the liquid in the theory would cause a significant discrepancy in predicting the bubble motion.

Acknowledgements—This work was supported in part by EPRI Grant Nos RP443-1 and RP443-2.

REFERENCES

BASSET, A. B. 1961 *Hydrodynamics*, p. 270. Dover, New York.

BATCHELOR, G. K. 1967 *An Introduction to Fluid Dynamics*, pp. 407–409. Cambridge Univ. Press, Cambs.

DREW, D. A. & LAHEY, R. T. JR 1987 The virtual mass and lift force on a sphere in rotating and straining inviscid flow. *Int. J. Multiphase Flow* **13,** 113–121.

HERRINGE, R. A. 1976 On the motion of small spheres in oscillating liquids. *Chem. Engng J.* **11,** 89–99.

KUO, J. T. 1978 Flow of bubbles through nozzles. Ph.D. Thesis, Thayer School of Engineering, Dartmouth College, Hanover, N.H.

LAHEY, R. T. JR 1977 Two-phase flow phenomena in nuclear reactor technology. RPI Research Project No. JBE43, Quarterly Progress Report (Dec.).

LAMB, H. 1972 *Hydrodynamics*, 6th edn, pp. 114, 273, 294. Dover, New York.

MORRISON, F. A. JR & STEWART, M. B. 1976 Small bubble motion in an accelerating liquid. *J. appl. Mech.* **Sept.,** 399–402.

MURRAY, J. D. 1965 On the mathematics of fluidization. *J. Fluid Mech.* **21,** 465–493.

SOO, S. L. 1967 *Fluid Dynamics of Multiphase Systems*, p. 262. Blaisdell, Waltham, Mass.

TEMKIN, S. & KIM, S. S. 1980 Droplet motion induced by weak shock waves. *J. Fluid Mech.* **96,** 133–157.

TOROBIN, L. B. & GAUVIN, W. H. 1961 The drag coefficient of single spheres moving in steady and accelerated motion in a turbulent fluid. *AIChE Jl* **7,** 615–619.

TYLER, A. L. & SALT, D. L. 1977 Periodic discontinuities in the acceleration of spheres in free flight. ASME Paper No. 77-WAIFE-3.

WALLIS, G. B. 1969 The separated flow regime of two-phase flow. Internal Report, Thayer School of Engineering, Dartmouth College, Hanover, N.H.

WALLIS, G. B. 1974 The terminal speed of single drops or bubbles in an infinite medium. *Int. J. Multiphase Flow* **1,** 491–511.

YEH, H. C. & YANG, W. J. 1968 Dynamics of bubbles moving in liquids with pressure gradient. *J. appl. Phys.* **39,** 3156–3165.